

# Unbiased Estimator for Distorted Conics in Camera Calibration

## Supplementary Material

### 7. Proof of Theorem and lemma in Sec. 4

#### 7.1. Proof of Theorem 1

*Proof.*

$$[x', y'] = D(x, y) = [f(x, y), g(x, y)] \quad (33)$$

$$\mathbf{J} = \text{Jacob}(D) = \begin{bmatrix} \frac{\partial f}{\partial x} & \frac{\partial f}{\partial y} \\ \frac{\partial g}{\partial x} & \frac{\partial g}{\partial y} \end{bmatrix}, \quad (34)$$

$$dA_{x'y'} = \sqrt{\det(\mathbf{G})} dA_{x'y'} = \sqrt{\det(\mathbf{J}^\top \mathbf{J})} dA_{x'y'} = \det(\mathbf{J}) dA_{x'y'}, \quad (35)$$

$$|A_{x'y'}| M_{x'y'}^{m,n} = \int (x')^m (y')^n dA_{x'y'}, \quad (36)$$

$$= \int f(x, y)^n g(x, y)^m \det(\mathbf{J}) dA_{xy}. \quad (37)$$

The positive definite matrix  $\mathbf{G}$  is called The First Fundamental Form or Riemannian Metric. Since  $f(x, y)$ ,  $g(x, y)$ , and  $\det(\mathbf{J})$  are polynomial functions of  $x$  and  $y$ ,  $M_{x'y'}^{n,m}$  can be expressed by a linear combination of  $M_{xy}^{i,j}$ .

$$|A_{x'y'}| M_f^{n,m} = \int \sum_{ij} c_{ij} x^i y^j dA_{xy} \quad (38)$$

$$= |A_{xy}| \left[ \frac{1}{|A_{xy}|} \int \sum_{ij} c_{ij} x^i y^j dA_{xy} \right] \quad (39)$$

$$= |A_{xy}| \sum_{ij} c_{ij} \left[ \frac{1}{|A_{xy}|} \int x^i y^j dA_{xy} \right] \quad (40)$$

$$= |A_{xy}| \sum_{i=0}^p \sum_{j=0}^q c_{ij} M_{xy}^{i,j}. \quad (41)$$

□

#### 7.2. Proof of Theorem 2

*Proof.*

$$x_n = \cos \alpha x_s - \sin \alpha y_s \quad (42)$$

$$y_n = \sin \alpha x_s + \cos \alpha y_s \quad (43)$$

$$s_n = x_n^2 + y_n^2 = x_s^2 + y_s^2 = s_s \quad (44)$$

$$\begin{aligned} dA_n &= \det(\mathbf{J}) dA_s \\ &= (\cos^2 \alpha + \sin^2 \alpha) dA_s = dA_s \end{aligned} \quad (45)$$

$$\therefore |A_n| = |A_s| \quad (46)$$

$$\mathbf{v}_n^r = \begin{bmatrix} \frac{1}{|A_n|} \int x_n s_n^r dA_n \\ \frac{1}{|A_n|} \int y_n s_n^r dA_n \\ \frac{1}{|A_n|} \int s_n^r dA_n \end{bmatrix} = \begin{bmatrix} \frac{1}{|A_s|} \int (\cos \alpha x_s - \sin \alpha y_s) s_s^r dA_s \\ \frac{1}{|A_s|} \int (\sin \alpha x_s + \cos \alpha y_s) s_s^r dA_s \\ \frac{1}{|A_s|} \int s_s^r dA_s \end{bmatrix} \quad (47)$$

$$= \begin{bmatrix} \cos \alpha & -\sin \alpha & 0 \\ \sin \alpha & \cos \alpha & 0 \\ 0 & 0 & 1 \end{bmatrix} \begin{bmatrix} \frac{1}{|A_s|} \int x_s s_s^r dA_s \\ \frac{1}{|A_s|} \int y_s s_s^r dA_s \\ \frac{1}{|A_s|} \int s_s^r dA_s \end{bmatrix} \quad (48)$$

□

### 7.3. Proof of Lemma 3

*Proof.*

$$I^{m,n} = \frac{1}{2\pi} \int_0^{2\pi} \cos^{m-1} \theta \cos \theta \sin^n \theta d\theta \quad (49)$$

$$= \frac{1}{2\pi} \left[ \frac{1}{n+1} \cos^{m-1} \theta \sin^{n+1} \theta \right]_0^{2\pi} + \frac{m-1}{n+1} \frac{1}{2\pi} \int \cos^{m-2} \theta \sin^{n+1} \theta \sin \theta d\theta \quad (50)$$

$$= \frac{m-1}{n+1} I^{m-2,n+2} \quad (51)$$

Similarly,

$$I^{m,n} = \frac{n-1}{m+1} I^{m+2,n-2} \quad (52)$$

By Eqs. (51) and (52), we can reduce m or n to zero or one. However,  $I^{1,n}$  and  $I^{m,1}$  is always zero as follows.

$$I^{1,n} = \frac{1}{2\pi} \int_0^{2\pi} \cos \theta \sin^n \theta d\theta = \left[ \frac{1}{n+1} \sin^{n+1} \theta \right]_0^{2\pi} = 0, \quad (53)$$

$$I^{m,1} = \frac{1}{2\pi} \int_0^{2\pi} \cos^m \theta \sin \theta d\theta = \left[ -\frac{1}{m+1} \cos^{m+1} \theta \right]_0^{2\pi} = 0. \quad (54)$$

Therefore, we only need to consider the even case when  $m$  is  $2i$  and  $n$  is  $2j$ . Otherwise,  $I^{m,n} = 0$ .  $I^{0,n}$  also has a reduction formula as

$$I^{0,n} = \frac{1}{2\pi} \int_0^{2\pi} \sin^n \theta d\theta = \frac{1}{2\pi} \int_0^{2\pi} \sin^{n-1} \theta \sin \theta d\theta \quad (55)$$

$$= \frac{1}{2\pi} \left[ -\cos \theta \sin^{n-1} \theta \right]_0^{2\pi} + \frac{n-1}{2\pi} \int_0^{2\pi} \sin^{n-2} \theta \cos^2 \theta d\theta \quad (56)$$

$$= \frac{n-1}{2\pi} \int_0^{2\pi} \sin^{n-2} \theta (1 - \sin^2 \theta) d\theta \quad (57)$$

$$= -(n-1)I^{0,n} + (n-1)I^{0,n-2}, \quad (58)$$

$$\therefore I^{0,n} = \frac{n-1}{n} I^{0,n-2}. \quad (59)$$

Using Eqs. (51) and (59), the analytic solution of  $I^{2i,2j}$  is obtained.

$$I^{2i,2j} = \frac{2i-1}{2j+1} \frac{2i-3}{2j+3} \dots \frac{1}{2j+2i-1} I^{0,2j+2i} \quad (60)$$

$$= \frac{2i-1}{2j+1} \frac{2i-3}{2j+3} \dots \frac{1}{2j+2i-1} \frac{2i+2j-1}{2i+2j} \frac{2i+2j-3}{2i+2j-2} \dots \frac{1}{2} \quad (61)$$

$$= \frac{(2i-1)(2i-3) \dots (1)(2j-1) \dots (1)}{(2i+2j)(2i+2j-2) \dots (2)} \quad (62)$$

$$= \frac{(2i-1)(2i-3) \dots (1)(2j-1) \dots (1)}{(2i+2j)(2i+2j-2) \dots (2)} \frac{(2i)(2i-2) \dots (2)(2j)(2j-2) \dots (2)}{(2i)(2i-2) \dots (2)(2j)(2j-2) \dots (2)} \quad (63)$$

$$= \frac{(2i)!(2j)!}{(i+j)!i!j!} \frac{1}{2^{2i+2j}} \quad (64)$$

The Eq. (64) is a symmetric equation of  $i$  and  $j$ . The factorial term such as  $(i+j)!$  readily induces numerically unstable; therefore, we convert the factorial term to a combination term such as  $\binom{i+j}{i}$ .

$$\frac{(2i)!(2j)!}{(i+j)!i!j!} \frac{1}{2^{2i+2j}} = \frac{(2i)!(2j)!}{(2i+2j)!} \frac{(2i+2j)!}{(i+j)!(i+j)!} \frac{(i+j)!}{i!j!} \frac{1}{2^{2i+2j}} = \frac{\binom{2i+2j}{i+j} \binom{i+j}{i}}{\binom{2i+2j}{2i} 2^{2i+2j}}. \quad (65)$$

Another advantage of combination terms is that we can develop a combination matrix in advance using Pascal's triangle.  $\square$

#### 7.4. Proof of Lemma 4

*Proof.*

$$x_0 = ar \cos \theta, \quad (66)$$

$$y_0 = br \sin \theta, \quad (67)$$

$$M_0^{m,n} = \frac{1}{\pi ab} \int x_0^m y_0^n dA_0 \quad (68)$$

$$= \int_0^{2\pi} \int_0^1 a^m b^n r^{m+n} \cos^m \theta \sin^n \theta rab dr d\theta \quad (69)$$

$$= \frac{a^{m+1} b^{n+1}}{\pi ab(m+n+2)} \int_0^{2\pi} \cos^m \theta \sin^n \theta d\theta \quad (70)$$

$$= \frac{a^m b^n}{1 + (m+n)/2} I^{m,n}. \quad (71)$$

□

#### 7.5. Proof of Theorem 5

*Proof.*

$$dA_s = dA_0, \quad (72)$$

$$\frac{1}{|A_s|} \int (x_s^2 + y_s^2)^r dA_s = \frac{1}{|A_s|} \sum_{k=0}^r \binom{r}{k} \int x_s^{2k} y_s^{2r-2k} dA_0 \quad (73)$$

$$= \frac{1}{|A_s|} \sum_{k=0}^r \binom{r}{k} \int (x_0 + t_x)^{2k} (y_0 + t_y)^{2r-2k} dA_0 \quad (74)$$

$$= \sum_{k=0}^r \binom{r}{k} \sum_{p=0}^{2k} \sum_{q=0}^{2r-2k} \binom{2k}{p} \binom{2r-2k}{q} t_x^{2k-p} t_y^{2r-2k-q} M_0^{pq} \quad (75)$$

$$= \sum_{p=0}^{2r} \sum_{q=0}^{2r-p} M_0^{pq} \sum_{k=\lceil p/2 \rceil}^{\lfloor r-q/2 \rfloor} \binom{r}{k} \binom{2k}{p} \binom{2r-2k}{q} t_x^{2k-p} t_y^{2r-2k-q} \quad (76)$$

Since  $M_0^{pq}$  is zero when  $p$  or  $q$  is odd number, we can rewrite the above equation using  $p = 2i$  and  $q = 2j$ . Using the above equations, we obtain Eqs. (77)–(79).

$$\mathbf{v}_s^r[2] = \frac{1}{|A_s|} \int (x_s^2 + y_s^2)^r dA_s = \sum_{i=0}^r \sum_{j=0}^{r-i} M_0^{2i,2j} \sum_{k=i}^{r-j} \binom{r}{k} \binom{2k}{2i} \binom{2r-2k}{2j} t_x^{2k-2i} t_y^{2r-2k-2j} \quad (77)$$

$$\begin{aligned} \mathbf{v}_s^r[0] &= \frac{1}{|A_s|} \int x_s (x_s^2 + y_s^2)^r dA_s = \frac{1}{|A_s|} \sum_{k=0}^{k=r} \binom{r}{k} \int (x_0 + t_x)^{2k+1} (y_0 + t_y)^{2r-2k} dA_0 \\ &= \sum_{k=0}^r \binom{r}{k} \sum_{p=0}^{2k+1} \sum_{q=0}^{2r-2k} \binom{2k+1}{p} \binom{2r-2k}{q} t_x^{2k-p+1} t_y^{2r-2k-q} M_0^{pq} \\ &= \sum_{i=0}^r \sum_{j=0}^{r-i} M_0^{2i,2j} \sum_{k=i}^{r-j} \binom{r}{k} \binom{2k+1}{2i} \binom{2r-2k}{2j} t_x^{2k-2i+1} t_y^{2r-2k-2j} \end{aligned} \quad (78)$$

Similarly,

$$\mathbf{v}_s^r[1] = \frac{1}{|A_s|} \int y_s (x_s^2 + y_s^2)^r dA_s = \sum_{i=0}^r \sum_{j=0}^{r-i} M_0^{2i,2j} \sum_{k=i}^{r-j} \binom{r}{k} \binom{2k}{2i} \binom{2r-2k+1}{2j} t_x^{2k-2i} t_y^{2r-2k-2j+1} \quad (79)$$

□

## 8. Derivation details

### 8.1. (Sec. 4.1) Geometric Feature of Ellipse

When the  $\mathbf{Q}$  represents an ellipse, the geometric features of the ellipse (i.e., center point and major/minor axis length) could be obtained from the matrix  $\mathbf{Q}$  as follows.

$$\mathbf{Q} \triangleq \begin{bmatrix} a & b & d \\ b & c & e \\ d & e & f \end{bmatrix} \quad (80)$$

$$h_1 = (ac - b^2), \quad (81)$$

$$h_2 = \sqrt{(a - c)^2 + 4b^2}, \quad (82)$$

$$t_x = (be - cd)/h_1, \quad (83)$$

$$t_y = (bd - ae)/h_1, \quad (84)$$

$$m_0 = \sqrt{\frac{2 \det(\mathbf{Q})}{h_1(a + c - h_2)}}, \quad (85)$$

$$m_1 = \sqrt{\frac{2 \det(\mathbf{Q})}{h_1(a + c + h_2)}}, \quad (86)$$

$$\alpha = \tan^{-1} \left( \frac{c - a + h_1}{-2b} \right). \quad (87)$$

Here,  $t_x$  and  $t_y$  are the center point of the ellipse, and  $m_0$  and  $m_1$  are the lengths of ellipse axes. The angle between the x-axis and the ellipse axis, whose length is  $m_0$ , is denoted as  $\alpha$  in Fig. 3

### 8.2. (Sec. 4.2) Tracking moment under distortion

The  $n_d$  is the number of distortion parameters defined in Eq. (11).

$$s = x_n^2 + y_n^2, \quad (88)$$

$$k = 1 + d_1 s + d_2 s^2 + d_3 s^3 + \dots + d_n s^n = \sum_{i=0}^{n_d} d_i s^i \quad (d_0 = 1), \quad (89)$$

$$x_d = k x_n \quad (90)$$

$$y_d = k y_n, \quad (91)$$

$$dA_d = \sqrt{\det(\mathbf{G})} dA_n \quad (92)$$

$$\sqrt{\det(\mathbf{G})} = \sqrt{\det(\mathbf{J}^T \mathbf{J})} = \det(\mathbf{J}) = \begin{vmatrix} \frac{\partial x_d}{\partial x_n} & \frac{\partial x_d}{\partial y_n} \\ \frac{\partial y_d}{\partial x_n} & \frac{\partial y_d}{\partial y_n} \end{vmatrix} \quad (93)$$

$$= \begin{vmatrix} k + 2x_n^2 \frac{\partial k}{\partial s} & 2x_n y_n \frac{\partial k}{\partial s} \\ 2x_n y_n \frac{\partial k}{\partial s} & k + 2y_n^2 \frac{\partial k}{\partial s} \end{vmatrix} = k(k + 2s \frac{\partial k}{\partial s}) = \sum_{i=0}^{n_d} d_i s^i \sum_{i=0}^{n_d} (2i + 1) d_i s^i. \quad (94)$$

Using the above equations, we obtain

$$\frac{|A_d|}{|A_n|} = \frac{1}{|A_n|} \int dA_d = \frac{1}{|A_n|} \int \sqrt{\det(\mathbf{G})} dA_n = \frac{1}{|A_n|} \int \left( \sum_{i=0}^{n_d} d_i s^i \right) \left( \sum_{i=0}^{n_d} (2i+1) d_i s^i \right) dA_n. \quad (95)$$

$$|A_d| M_d^{1,0} = \int x_d dA_d = \int k x_n \sqrt{\det(\mathbf{G})} dA_n = \int x_n k^2 \left( k + 2s \frac{\partial k}{\partial s} \right) dA_n \quad (96)$$

$$M_d^{1,0} = \frac{|A_n|}{|A_d|} \frac{1}{|A_n|} \int x_n \left( \sum_{i=0}^{n_d} d_i s^i \right)^2 \left( \sum_{i=0}^{n_d} (2i+1) d_i s^i \right) dA_n. \quad (97)$$

$$|A_d| M_d^{0,1} = \int y_d dA_d = \int y_n k^2 \left( k + 2s \frac{\partial k}{\partial s} \right) dA_n, \quad (98)$$

$$M_d^{0,1} = \frac{|A_n|}{|A_d|} \frac{1}{|A_n|} \int y_n \left( \sum_{i=0}^{n_d} d_i s^i \right)^2 \left( \sum_{i=0}^{n_d} (2i+1) d_i s^i \right) dA_n. \quad (99)$$

We can reduce the computational cost as follows.

$$\left( \sum_{i=0}^{n_d} d_i s^i \right) \left( \sum_{i=0}^{n_d} (2i+1) d_i s^i \right) = \sum_{i=0}^{n_d} \sum_{j=0}^{n_d} (2i+1) d_i d_j s^{i+j} \quad (100)$$

$$= \sum_{r=0}^{2n_d} w_{0r} \cdot s^r, \quad \left( w_{0r} = \sum_{i=\max(0, r-n_d)}^{\min(r, n_d)} (2i+1) d_i d_{r-i} \right) \quad (101)$$

$$\left( \sum_{i=0}^{n_d} d_i s^i \right)^2 \left( \sum_{i=0}^{n_d} (2i+1) d_i s^i \right) = \sum_{i,j,k=0}^{n_d} (2i+1) d_i d_j d_k s^{i+j+k} \quad (102)$$

$$= \sum_{r=0}^{3n_d} w_{1r} \cdot s^r \quad \left( w_{1r} = \sum_{i=\max(0, r-2n_d)}^{\min(r, n_d)} (2i+1) d_i \sum_{j=\max(0, r-i-n_d)}^{\min(r-i, n_d)} d_j d_{r-i-j} \right) \quad (103)$$

Then, Eqs. (95) to (99) are rewritten as

$$\frac{|A_d|}{|A_n|} = \sum_{r=0}^{2n_d} w_{0r} \left[ \frac{1}{|A_n|} \int s^r dA_n \right] \quad (104)$$

$$M_d^{1,0} = \frac{|A_n|}{|A_d|} \sum_{r=0}^{3n_d} w_{1r} \left[ \frac{1}{|A_n|} \int x_n s^r dA_n \right] \quad (105)$$

$$M_d^{0,1} = \frac{|A_n|}{|A_d|} \sum_{r=0}^{3n_d} w_{1r} \left[ \frac{1}{|A_n|} \int y_n s^r dA_n \right] \quad (106)$$

### 8.3. (Sec. 4.2) The centroid of the distorted ellipse on the image plane

$$\begin{bmatrix} x_i \\ y_i \end{bmatrix} = \begin{bmatrix} f_x & \eta & c_x \\ 0 & f_y & c_y \end{bmatrix} \begin{bmatrix} x_d \\ y_d \\ 1 \end{bmatrix} \quad (107)$$

$$\det(\mathbf{J}) = \begin{vmatrix} f_x & \eta \\ 0 & f_y \end{vmatrix} = f_x f_y, \quad (108)$$

$$|A_i| = f_x f_y |A_d|, \quad (109)$$

$$\bar{x}_i \triangleq M_i^{1,0} = \frac{1}{|A_i|} \int x_i dA_i = \frac{|A_d|}{|A_i|} \frac{1}{|A_d|} \int (f_x x_d + \eta y_d + c_x) f_x f_y dA_d \quad (110)$$

$$= f_x M_d^{1,0} + \eta M_d^{0,1} + c_x \quad (\because |A_i| = f_x f_y |A_d|), \quad (111)$$

$$\bar{y}_i \triangleq M_i^{0,1} = f_y M_d^{0,1} + c_y, \quad (112)$$

$$\begin{bmatrix} \bar{x}_i \\ \bar{y}_i \end{bmatrix} = \begin{bmatrix} f_x & \eta & c_x \\ 0 & f_y & c_y \end{bmatrix} \begin{bmatrix} \bar{x}_d \\ \bar{y}_d \\ 1 \end{bmatrix}. \quad (113)$$

### 8.4. Robustness of the first moment

As mentioned at Sec. 4.1, a conic is defined with second-order moments. Using the above results, it is possible to calculate the second-order moments of distorted conic in the image plane. However, the boundary blur effects easily contaminate high-order moments. For instance, if there is some dilation or erosion in the ellipse, the major and minor axis lengths become shorter or longer while the centroid of the shape is invariant. For calibration, the unbiased estimator and accurate measurement are both essential; therefore, utilizing only the first momentum is more beneficial for accurate calibration. Another advantage of the first moment is its robustness to the image noise. Assume that there is some noise in the boundary points of the shape and the noise follows a normal distribution whose mean is zero and variance is  $\sigma^2$ , then the variance of the first moment of the shape is reduced by  $1/n$ . For boundary points following  $X_i \sim \mathcal{N}(\mu, \sigma^2)$ ,

$$M_X^1 = \frac{1}{n} \sum_i X_i \quad (\text{first moment}) \quad (114)$$

$$\begin{aligned} \text{Var}(M_X^1) &= \text{Var}\left(\frac{1}{n} \sum_i X_i\right) \quad (115) \\ &= \frac{1}{n^2} \text{Var}\left(\sum_i X_i\right) = \frac{n \text{Var}(X_i)}{n^2} = \frac{\sigma^2}{n}. \end{aligned}$$

This is one of the reasons why the circular pattern is more robust to the boundary blur effect than the checkerboard, whose control points are directly obtained from the single point. This finding will be demonstrated via a set of experiments in Sec. 5.1.

## 9. Experiments details

### 9.1. Characteristics of TIR camera

The thermal infrared (TIR) camera is a distinctive vision sensor for extreme environments. The TIR camera is limited in recognizing colored patterns because it distinguishes objects by infrared energy, not by color; hence, a TIR camera needs a particular target for calibration. Some thermal-specific calibration targets in the literature include a printed circuit board (PCB) composed of different heat conductivity squares [24]. However, even with this target, achieving high calibration accuracy is onerous. The thermal images often include low resolution, high distortion, and blunt boundaries, possibly leading to inaccurate control point detection. For example, the temperature discrepancy between two adjacent objects is decreased by conduction and radiation. This phenomenon causes blunt boundaries as illustrated in Fig. 7.

### 9.2. Vector representation of reprojection errors on the RGB image

We visualized the reprojection error per the actual distance from the camera to the calibration target in Fig. 5. To provide more intuition about the distribution in spatial aspect, we performed the calibration using 20 images and scattered the reprojection

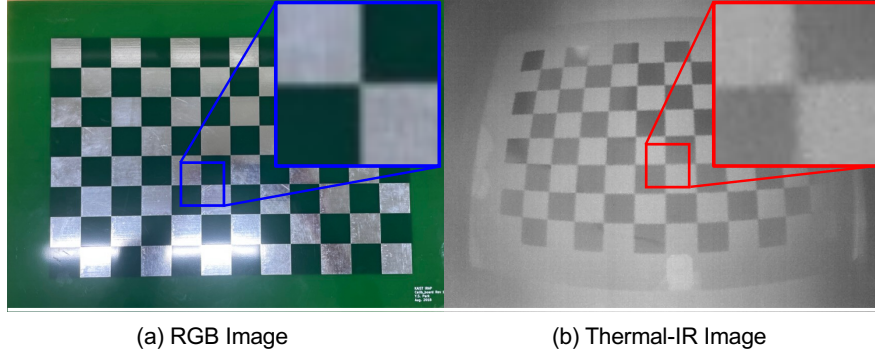


Figure 7. **The checkerboard pattern captured from the RGB camera (left) and TIR camera (right).** Compared to RGB images, the boundary is highly blunt when captured from TIR. Severe distortion can also be observed in the thermal images

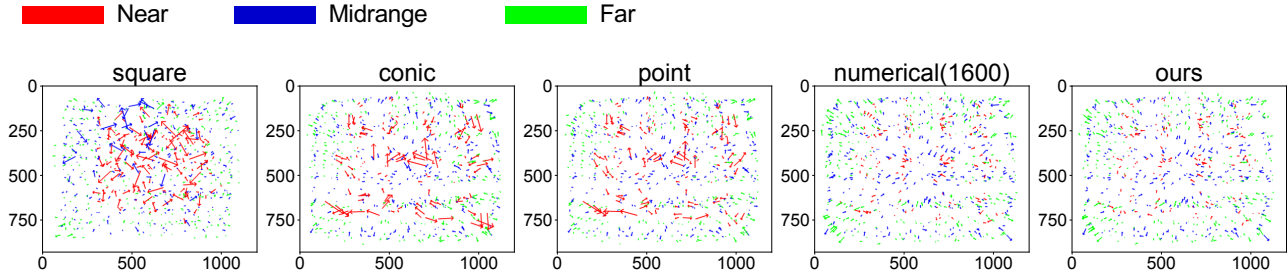


Figure 8. **Visualization of reprojection error vector.** We collected 60 images and scattered 720 reprojection error vectors of the control points on the image plane. While our method shows low reprojection error across the entire image area, other methods include larger error vectors. For visualization, the error vectors are scaled up 50 times.

error vector on the image plane. Fig. 8 is the result obtained by repeating this procedure three times. In our method, it is observed that the magnitude of the error vector remains small regardless of the depth or 2D position in the image. In contrast, significantly larger error vectors are observed at closer distances for the checkerboard pattern. This phenomenon results from the measurement noise of control points, which increases at closer distances. For the remaining two methods based on circular patterns (i.e. conic-based and point-based), locally consistent large error vectors are observed. This local consistency indicates that these error vectors stem from the estimator’s bias rather than measurement noise.

### 9.3. Analytic solution of $T_t^o$ and $T_c^m$

$$\mathbf{X} = \mathbf{T}_t^o, \tag{116}$$

$$\mathbf{Y} = \mathbf{T}_c^m, \tag{117}$$

$$\mathbf{T}_{o_i}^m \mathbf{X} = \mathbf{Y} \mathbf{T}_{t_i}^c \tag{118}$$

For obtaining optimal solution of  $\mathbf{X}$  and  $\mathbf{Y}$ , we first decouple  $\mathbf{X}$  and  $\mathbf{Y}$  using Eq. (118) as

$$(\mathbf{T}_{o_j}^m)^{-1} \mathbf{T}_{o_i}^m \mathbf{X} = \mathbf{X} (\mathbf{T}_{t_j}^c)^{-1} \mathbf{T}_{t_i}^c \tag{119}$$

$$\mathbf{T}_{o_j}^m (\mathbf{T}_{o_i}^m)^{-1} \mathbf{Y} = \mathbf{Y} \mathbf{T}_{t_j}^c (\mathbf{T}_{t_i}^c)^{-1} \tag{120}$$

Therefore, the remaining part is to solve the  $A_i X = X B_i$  problem for  $i = 1 \sim n$ . According to the paper [21], this problem has a closed-form solution.

$$X = \begin{bmatrix} R_x & t_x \\ \mathbf{0}^\top & 1 \end{bmatrix} = \begin{bmatrix} \exp([\mathbf{w}_x]) & t_x \\ \mathbf{0}^\top & 1 \end{bmatrix}, \quad (121)$$

$$A_i = \begin{bmatrix} \exp([\mathbf{w}_{a_i}]) & t_{a_i} \\ \mathbf{0}^\top & 1 \end{bmatrix} \quad B_i = \begin{bmatrix} \exp([\mathbf{w}_{b_i}]) & t_{b_i} \\ \mathbf{0}^\top & 1 \end{bmatrix}, \quad (122)$$

$$P = \sum_i \mathbf{w}_{b_i} \mathbf{w}_{a_i}^\top, \quad (123)$$

$$\hat{R}_x = (M^\top M)^{-1/2} M^\top, \quad (124)$$

$$C = \begin{bmatrix} I - R_{a_1} \\ I - R_{a_2} \\ \dots \\ I - R_{a_n} \end{bmatrix}, \quad d = \begin{bmatrix} t_{a_1} - \hat{R}_x t_{b_1} \\ t_{a_2} - \hat{R}_x t_{b_2} \\ \dots \\ t_{a_n} - \hat{R}_x t_{b_n} \end{bmatrix}, \quad (125)$$

$$\hat{t}_x = (C^\top C)^{-1} C^\top d. \quad (126)$$